Thermal Science and Engineering Progress 67 (2025) 104175

Contents lists available at ScienceDirect

Thermal Science and Engineering Progress

journal homepage: www.sciencedirect.com/journal/thermal-science-and-engineering-progress

Comparative analysis of image segmentation methods on various flame types and their influence on flame stability assessment

Mohsen Gharib [a,*], Markus Vogelbacher [b], Jörg Matthes [b], Martin Gräbner [a,c], Andreas Richter [a,c]

[a] Fraunhofer Institute for Ceramic Technologies and Systems, Winterbergstr. 28, 01277 Dresden, Germany
[b] Institute for Automation and Applied Informatics, Karlsruhe Institute of Technology, Hermann-von-Helmholtz-Platz 1, 76344 Eggenstein-Leopoldshafen, Germany
[c] Institute of Energy Process Engineering and Chemical Engineering, TU Bergakademie Freiberg, Fuchsmühlenweg 9 D, 09599 Freiberg, Germany

ARTICLE INFO

Keywords:
Flame characteristics
Image segmentation
Gasification
Flame stability
Process monitoring

ABSTRACT

Image-based flame diagnostics are crucial in optimizing high-temperature processes, improving efficiency, and minimizing harmful emissions. A pivotal step in this process is flame segmentation. Despite its importance, there is a lack of studies examining the segmentation of low-brightness flames. In many industrial scenarios, flame images suffer from challenges such as blurry boundaries and inadequate brightness. Therefore, in this study, different segmentation techniques were explored. To assess the robustness of each method, flames from three distinct feedstocks were optically observed within a multi-feed test facility. Various techniques were evaluated, including Otsu's method, manual thresholding, multilevel thresholding, k-nearest neighbors (KNN), and deep learning (U-Net). Then, geometrical and positional flame characteristics were derived. It was found that, in low-brightness flame scenarios, classic methods tend to produce inaccurate results, with a segmentation quality of 60–67 %. Furthermore, additional image preprocessing steps are necessary to effectively segment such flames to enhance the flame's appearance. U-Net emerged as the most promising among the tested methods, achieving a segmentation quality of around 89 % for low-brightness flames. Although it provided nearly accurate flame shapes, aligning well with the ground truth. Furthermore, a new approach was introduced to estimate global flame stability by considering factors such as flame orientation, ignition point, and geometric parameters, thereby enabling a comprehensive stability assessment. It was observed that solid fuel flames exhibited the highest stability index, around 98 %. Additionally, it was evident that inaccuracies in segmentation quality significantly impacted the stability index, highlighting the importance of robust segmentation steps in flame stability assessment.

1. Introduction

Flame monitoring systems are crucial in controlling the process, ensuring optimal efficiency and safety by continuously assessing and adjusting operational parameters. Inside the reactor, the reactions take place under elevated temperatures and pressures. This restricts access to the reaction chamber, which makes physical measurements difficult [1]. The use of imaging technologies with flames is essential since it allows for non-intrusive flame monitoring and visualization. The first and most crucial step of flame analysis is image segmentation, which identifies the region of the thermochemical reaction [2,3].

As a result, excellent segmentation quality leads to the extraction of highly accurate results while simultaneously reducing data processing time [4]. However, in most situations, the visual appearance of flames frequently lacks optimal quality, presenting a challenge in extracting flame characteristics, such as shape and stability. Many studies previously reported the feasibility of using image processing techniques not only in flame monitoring systems [5,6,7,8], but also in online fuel characterization [9] and hydrocarbons' characteristics predictions [10]. However, most of them concentrate on just one aspect of the overall analysis, such as developing new methods for better flame segmentation [3,11,12,13] or extracting and evaluating flame characteristics after changing some operating parameters [14,15]. Therefore, this study aims to focus on the entire flame analysis process. It goes beyond basic image processing by comparing various segmentation techniques applied to flames from different fuel types (natural gas, coal, and diesel) and introducing a new method for flame stability assessment based on the

* Corresponding author.
E-mail address: Mohsen.Gharib@iec.tu-freiberg.de (M. Gharib).

https://doi.org/10.1016/j.tsep.2025.104175
Received 24 March 2025; Received in revised form 1 October 2025; Accepted 2 October 2025
Available online 5 October 2025

Nomenclature

$\overline{L_i}$	Average lift-off distance per frame
$\overline{\theta_i}$	Average deviation angle per frame
$\overline{\Delta P}$	Normalized average change
Δp_i	Absolute percentage change
L	Total number of intensity levels
$L_{\max}$	Maximum lift-off
N	Number of frames
$P(i)$	Probability of occurrence of intensity level
T	Threshold
$T_{\min}$	Minimum threshold
w_{a}	Area weight
w_{dev}	Deviation angle weight
w_{geometry}	Geometry weight
w_{h}	Height weight
w_{liftoff}	Lift-off distance weight
w_{w}	Width weight
$\theta_{\max}$	Maximum deviation angle
$\mu_1(T)$	Mean intensity of the pixel in classes 1
μ_j	Centroid of cluster j
$\mu_{\mathrm{o}}(T)$	Mean intensity of the pixel in classes 0
$\omega_1(T)$	Probabilities of pixels assigned to the object
$\omega_{\mathrm{o}}(T)$	Probabilities of pixels assigned to the background
$\sigma^2(T)$	Total variance

Abbreviations

DASI	Deviation angle stability index
GSI	Geometry stability index
IoU	Intersection over Union
KNN	k-nearest neighbors
LOSI	Lift-off stability index
ML	Machine learning
MSE	Mean squared error
ROI	Region of interest
RMSE	Root mean squared error

extracted features. Additionally, the relationship between segmentation quality and its impact on flame stability outcomes was investigated.

The previous research can be categorized into two groups. The first group focuses on flame image segmentation methods, primarily aiming to detect flame edges. One notable application of such methods is in fire detection surveillance systems, as evidenced by studies such as [16,17,18,19]. In [20], different image processing segmentation techniques and machine learning models were compared. The aim was to segment the radiation zones within the flame to provide risk management, and it was proved that deep learning techniques provide better performance than traditional image processing methods. Besides, Qiu et al. [3] introduced a new edge detection algorithm, which was compared against well-known edge detection algorithms. This algorithm showed accurate results in terms of identifying flame edges. Yan et al. [11] presented an innovative flame image segmentation method by dividing the flame image into small stripes, segmenting them, and finally reconstructing them into a whole image again. This method provided better flame image segmentation accuracy when compared with the Canny edge detector and Otsu's thresholding method. Another approach for flame image segmentation based on pseudo-color enhancement was proposed by Fan et al. [21]. This method was sufficient to detect the flame borders and estimate the flame shape.

By looking at one important characteristic of flames, their turbulent motion, some researchers started segmenting the flame based on motion. A previous study proposed a flame image segmentation based on the salience of motion and color [22]. This model showed high accuracy in segmenting the flame area. The concept is straightforward: find the moving object in a video or image series, and it will be the flame. Großkopf et al. [23] investigated the potential of using neural networks for segmentation results of overlapping flames. The study showed that NNs can be used in the context of closed-loop combustion process control to leverage process capability and energy efficiency. Indeed, most of the above-mentioned and the existing flame detection methods produce accurate results, but only when the images are of high quality. The segmentation task becomes more difficult with those methods when the flame borders are not visible, such as in time-averaged images or low-brightness flames. Consequently, another approach to solve this problem is required. For that reason, the initial objective of this study is to identify the most robust approach for segmenting flame images of varying quality.

The second research group concentrates on extraction flame characteristics, firstly, flame shape such as length [24,25,26], burning velocity [27], and stability [5,28]. There is no preferred definition of flame length. It can, however, be defined as the average longitudinal extension of the flame [29]. Yang et al. [30] investigated how the length and volume of liquefied propane gas flame changes with the oxidizer temperature at various oxygen concentrations. Another study examined the relation between the flame length and a high initial discharging velocity when the fuel-release time and mass flow rate of fuel were varied [14]. Xi et al. [31] demonstrated that the flame length grows as the fuel mass flow rate increases and that the nozzle exit velocity has no effect. Accordingly, the flame length indicates several variables, such as oxidizer and fuel mass flow rate or temperature. With image processing techniques, different approaches for measuring the flame length were proposed [21,32]. Richter et al. [1] employed optical measurements to study the flame structure, which was used to validate numerical results. Wang et al. [33] applied an image-processing method to identify abnormal combustion situations in gas-fired combustion. Nevertheless, in prior studies, the flame borders were consistently and accurately detected, facilitating the straightforward estimation of visual flame dimensions.

Flame stability is also a significant factor that can be estimated from the flame images. Controlling flame stability is critical for safer and more efficient processes, ensuring optimum energy conversion and reducing emissions. Neural networks were used previously to detect flame instabilities from the flame images [34,35]. Han et al. [36] introduced an autoencoder deep neural network to detect flame instabilities through flame images which overcomes the shortcomings of the traditional techniques. Flame oscillation, commonly known as 'flickering,' is one of the most important indicators of flame instability. Therefore, measuring it has long been of interest [37]. Many approaches have been proposed to measure flame flickering [38]. Ying-chun et al. [39] proved that the moment function of a flame image can represent flame oscillation. In another study, a method was developed to segment the fire images based on finding a quantitative relation between R, G, and B values of the fire pixels and then studied the oscillation feature [18]. The oscillatory characteristics of pulverized coal flames have been estimated using image processing and spectral analysis across different areas of the flame [40]. Various methods exist for assessing flame stability, such as the online flame stability monitoring system developed by Matthes et al. [41]. This system calculates the flame stability index by comparing flame areas in successive images. However, a general stability index that includes various flame characteristics is still required. Our study's second objective is to develop a comprehensive stability index encompassing all flame characteristics extracted during the segmentation process. These characteristics include flame geometrical

Table 1
Technical data of the test facility.

Data	Value	Unit
Burner power	1000	KW
Solid fuel flowrate (coal)	130	Kg/h
Liquid fuel flowrate (diesel)	65	Kg/h
Gas fuel flowrate (natural gas)	75	Nm^3/h
Operating pressure	50	mbar g
Maximum operating temperature	1400	°C
Quench temperature	80-90	°C

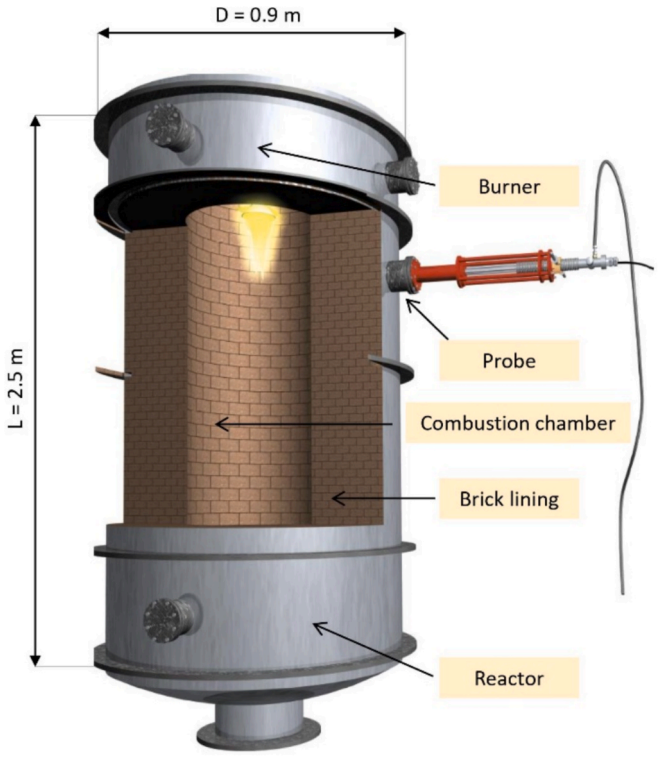

Fig. 1. The reactor with the optical probe [5].

parameters, ignition point, and deviation angle. Furthermore, the influence of segmentation quality is investigated on flame stability results. This step is crucial, as it ensures the accuracy and reliability of our stability assessments.

This work covers two aspects of flame image analysis: a comprehensive investigation of flame segmentation algorithms and the extraction of flame characteristics, including geometric features and stability assessment. The aim is to evaluate different segmentation algorithms for non-ideal flame images from three different feedstocks and to establish a comprehensive flame analysis workflow. The workflow is designed to be adaptable for future use with alternative fuels, such as hydrogen or ammonia, and to provide a robust basis for ongoing research into combustion and gasification processes. To achieve this, both traditional image processing techniques and advanced deep learning methods have been used for flame segmentation, ensuring a versatile and effective approach. Flame characteristics, including flame length, maximum width, and deviation angle, were then derived from the segmentation results. Furthermore, a new approach is introduced to estimate the global flame stability based on the flame orientation, ignition point, and geometric parameters, providing a comprehensive stability assessment.

The novelty of this work lies in two key contributions: first, the systematic evaluation of flame segmentation methods under challenging low-brightness and low-contrast flame conditions, which are commonly

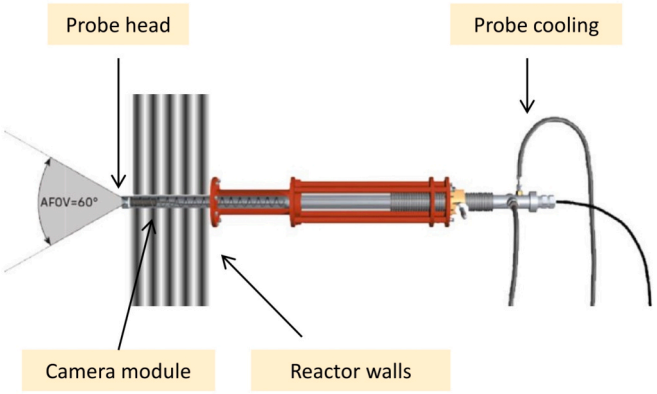

Fig. 2. The optical probe system attached to the combustion chamber.

encountered in industrial environments but are underrepresented in the literature. This challenge is tackled using our hybrid U-Net-based solution. Secondly, the introduction of a new integrated flame stability assessment framework that combines geometric, positional, and angular features using a weighted stability index. This index offers a more flexible and comprehensive alternative to traditional stability metrics that rely on individual parameters or fixed assumptions. The structure of this work is as follows: Section 2 describes the experimental setup, Section 3 details the methods and approaches for flame segmentation and feature extraction, and Section 4 presents the results and discussions.

2. Experimental setup

2.1. Multi-feed test facility

In this work, a multi-feed test facility with an applicable optical diagnostic system was designed to monitor the flames from different feedstocks. The core element of the test facility is a 1 MW reaction chamber, which is provided with a refractory lining. The reactor has multiple additional nozzles specifically designed for mounting optical measuring devices. The system was designed to use and test different burners for different feedstocks, focusing on the optical evaluation of multiple flames depending on the feed material. Table 1 lists the relevant operational parameters. The combustion chamber is shown in Fig. 1. It consists of ports for the pilot and main burners and 16 optical ports for optical measurements (at five different planes). The combustion chamber contains a 250 mm thick refractory lining inserted after installing the steel jacket. During operation, the reaction temperature is around 1200 °C, with a maximum of 1400 °C.

2.2. The optical system

The optical probe system was developed and installed to observe the flame. This system makes it possible to carry out an optical diagnosis of the primary oxidation of solid, liquid, and gas reactions in atmospheric and pressurized environments. It can operate at a maximum permissible pressure of 10 bar for the flushing, cooling, and camera compartments. The system can handle high temperatures, with a maximum allowable operating temperature of 1500 °C in the reaction chamber. The probe has a maximum outer diameter of 45 mm. In comparison, the endoscope system within the probe has a maximum outer diameter of 28 mm to accommodate the internal cooling system. The cooled probe head is designed to penetrate up to 50 mm into the reaction chamber. The optical probe incorporates advanced technical solutions, including an airlock system, pressure equalization, a sealing system, and a cooling and rinsing system to ensure performance and safety.

The probe cooling system consists of a double-walled cooling jacket.

Table 2
Overview of the test runs.

Case	Burner 1	Burner 2	Feedstock	O_2 / air Nm^3/h	Natural gas Nm^3/h	Coal Kg/h	Diesel Kg/h	Frequency Hz
1	✓	–	Gas (natural gas)	64.5	63	–	–	1000
2	✓	–	Solid (coal)	61.2	20	90	–	1000
3	–	✓	Liquid (diesel)	120	–	–	11	1000

A guide coil runs between the inner and outer jackets, separating the coolant supply and return. The probe head is a welded assembly made from several machined parts, including a viewing glass holder that secures and seals the glass while distributing nitrogen to keep it clear. The cooling water is also redirected within the probe head. At the probe tip, nitrogen is directed to the viewing glass, providing cooling and protection from dirt particles.

The probe system can be mounted on one of the 16 optical ports of the test facility (see Fig. 2). This system is connected to a high-speed camera (Phantom v1840) to acquire flame images, which can capture videos at (1000–10000) Hz. In our study, the flame videos were captured at 1000 Hz. The resolution of the camera was 1280 × 800 pixels, and the exposure time was set to 10 μs to capture detailed flame dynamics without motion blur. A spatial calibration was performed, with an approximate resolution of 1.29 mm/pixel in both horizontal and vertical directions. The image signal is transmitted from the probe via an endoscope, as the design does not include a camera at the probe head. The rear end of the probe has a pipe fitting for attaching the endoscope or for attaching pressure-resistant pipes. The endoscope can observe the flame visually or with a camera. The same optical port and camera parameters were used for all flame types to ensure consistent viewing conditions and comparability across the test cases. The system was validated in extended campaigns using coal, diesel, and natural gas fuels, during which the optical probe maintained a clear viewing window for over 6 h (gas, diesel) and over 9 h (coal), with negligible fouling, confirming the effectiveness of the nitrogen cleaning system.

2.3. Test series

In this work, various test experiments were carried out to test and evaluate the gasification of different feedstocks. There were more than sixty cases in these experiments with different operating conditions (fuel type, oxidation amount, fuel amount, and burner type). However, only three representative cases were selected for the analysis in this study. As several tests were excluded, either for optical system calibration or due to unstable or unclear flame formation. Among the valid cases, some exhibited similar characteristics within each fuel category. Thus, one stable and visually representative case per fuel type was chosen to ensure diversity in flame types while avoiding redundancy.

Table 2 summarizes the specific operating conditions applied during the flame recording experiments for each fuel type. These values represent the actual fuel and oxidizer flowrates, burner configuration, and measurement conditions used during high-speed imaging. However, it is important to note that the experiments were not designed as a parametric study to analyze the influence of operating conditions on flame behavior. Instead, the primary aim was to commission the test facility and calibrate the optical system. The tested fuels and operating conditions were: natural gas with oxygen (max. thermal power ~ 700 kW, reactor temperature 1250–1350 °C), diesel with air (120 kW, 850–900 °C), and pulverized coal with oxygen (1000 kW, 1300–1400 °C). All tests were conducted under fuel-rich (reducing) conditions, except for the oil flame, which was operated in both reducing and slightly oxidizing modes.

The gas and solid fuel tests were carried out with a multi-feed burner (Burner 1), which can be operated with either a swirled primary gasification fuel inlet or an annular secondary gasification fuel inlet. This burner is suitable for gaseous fuels injected via a lateral inlet and for solid fuels injected via the axial inlet. For the liquid fuel tests, an oil burner (Burner 2) was used, and the fuel was atomized through a nozzle with an oil pre-pressure of approximately 8 bar. Air was used as the oxidizing agent.

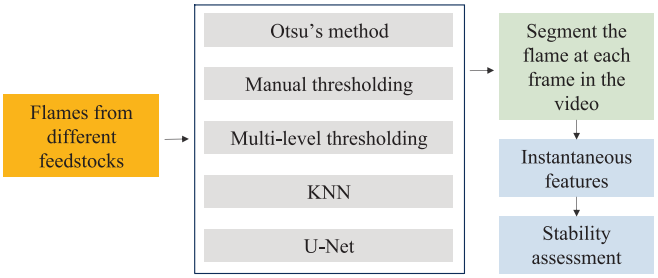

Fig. 3. Workflow of the image segmentation method evaluation.

3. Methodology

In this study, various segmentation techniques derived from image processing and deep learning methods were applied, as shown in Fig. 3. The use of well-established methods for flame segmentation in this work is intended for comparison purposes, specifically to assess how effectively these techniques perform when applied to low-brightness flame images. Subsequently, the study focuses on extracting instantaneous flame features. A comparative analysis was performed to determine each flame type's optimal segmentation, followed by a comprehensive stability assessment based on the extracted flame characteristics. The upcoming section provides a detailed overview of each method and explains the flame characteristics extraction process.

3.1. Segmentation techniques

3.1.1. Manual thresholding

Manual thresholding is the first and most straightforward method for image segmentation [42]. In this technique, a single threshold, called T_{min}, is manually applied to partition the entire image. This threshold is uniformly applied to all pixels within the flame image. Pixels with values below T_{min} are assigned a zero value, corresponding to the background, while those above are designated as the object, as detailed in Equation (1). Consequently, the outcome is two distinct regions: object and background.

$$g(x,y) = \begin{cases} 1 \text{ if } f(x,y) > T_{min} \\ 0 \text{ if } f(x,y) \le T_{min} \end{cases} \quad (1)$$

where $f(x, y)$ represents the gray level of the pixel at the coordinates (x, y). The implementation of this method is challenging when applied to most flame images; this difficulty arises when there is insufficient contrast between the background and the flame [43,44]. In such cases, the contours of the flame may not be clearly defined, making accurate detection difficult. This is because this method requires the image to have a bimodal histogram to extract the object.

3.1.2. Automatic thresholding (Otsu's method)

The second approach that caught our attention in this study was

Otsu's thresholding method, developed by Otsu et al. in 1979 [45]. This algorithm returns a single intensity value that separates the image into two classes, object, and background, because of the dynamic and automatic determination of the threshold value. This method has been used extensively in flame image-related applications [46,47,48,49]. However, it has some limitations because the image histogram needs a bimodal distribution (two clear peaks) to find the optimum threshold value between those peaks. Mathematically, Otsu's method can be expressed as follows:

Let $P(i)$ be the probability of occurrence of intensity level i in the image, and $\omega_o(T)$ and $\omega_1(T)$ represent the probabilities of pixels assigned to classes 0 (background) and 1 (object) based on the threshold T, respectively. The total variance $\sigma^2(T)$ is given by:

$$\sigma^2(T) = \omega_o(T) \cdot \omega_1(T) \cdot [\mu_o(T) - \mu_1(T)]^2 \quad (2)$$

where $\mu_o(T)$ and $\mu_1(T)$ are the mean intensities of the pixel in classes 0 and 1 respectively. The probabilities $\omega_o(T)$ and $\omega_1(T)$ are calculated as:

$$\omega_o(T) = \sum_{i=0}^{t} P(i) \quad (3)$$

$$\omega_1(T) = \sum_{i=t+1}^{L-1} P(i) \quad (4)$$

where L is the total number of intensity levels in the image. The optimal threshold is determined by maximizing $\sigma^2(T)$ across all possible threshold values. In this study, Otsu's method was applied to a predetermined region of interest (ROI), which is manually selected to reduce the influence of irrelevant background or noise. This can lead to more accurate thresholding results.

3.1.3. Multi-level thresholding

The third approach is multi-level thresholding, a segmentation technique that extends the concept of image thresholding (used in the previous two approaches) beyond the binary pixel classification [50]. In contrast to traditional thresholding methods that divide the image into two regions (foreground and background), multi-level thresholding involves partitioning an image into multiple intensity-based classes. This approach is particularly valuable in scenarios where an image exhibits complex intensity variations, and a single threshold is insufficient to capture the details of different objects or regions, such as flame images. The multi-level thresholding aims to identify and assign pixels to several intensity levels, thereby allowing for a more detailed representation of the underlying image structure. Various algorithms for multi-level thresholding exist, each aiming to optimize the partitioning of pixels into distinct classes based on statistical properties or optimization criteria [51]. These techniques work well for flame images with varying content by using multiple thresholds. Therefore, multi-level thresholding methods can be more adaptable to these changes than single-level thresholding, as they allow for segmenting different intensity levels at each time point. This study used three threshold values, and the flame region was determined visually.

3.1.4. K-Nearest neighbors (KNN)

The K-Nearest Neighbors (KNN) segmentation method used in our study is another robust flame segmentation approach [20,52]. As a supervised learning algorithm, KNN classifies pixels based on the majority class of their k-nearest neighbors. In the context of flame segmentation, each pixel's class (flame or background) is determined by examining the classes of its neighboring pixels. Unlike traditional methods, KNN does not assume a specific underlying distribution of pixel intensities, making it remarkably flexible for various image types.

Mathematically, the KNN algorithm involves the identification of k-nearest neighbors for each pixel, where 'k' is a user-defined parameter [53]. The pixel is then assigned to the class that is most prevalent among its neighbors, following the equations:

$$\text{label}(x_i) = \text{argmin}_j \|x_i - \mu_j\|^2 \quad (5)$$

$$\mu_j = \frac{1}{|C_j|} \sum_{x_i \in C_j} x_i \quad (6)$$

In these equations, label (x_i) represents the assigned cluster label for the pixel x_i. μ_j denotes the centroid of the cluster j, calculated as the mean of the data points within a cluster j. C_j signifies the set of data points assigned to cluster j. $\|x_i - \mu_j\|^2$ denotes the Euclidean distance between pixel x_i and the centroid μ_j. The term argmin$_j$ signifies the index corresponding to the minimum value, determining the cluster label.

This process is repeated for all pixels in the image, resulting in a segmented image where each pixel is labeled based on the majority class within its local neighborhood. The algorithm's efficiency depends on the appropriate choice of the 'k' parameter, which influences the size of the pixel neighborhood considered during classification.

3.1.5. Neural networks (U-Net)

The final method used in this study is the U-Net model, which is well-regarded for its effectiveness in image segmentation tasks [54]. U-Net has received considerable attention for its ability to accurately segment images by employing a distinctive design that combines a contracting path for feature extraction with an expansive path for precise localization. This architecture has consistently demonstrated high performance in flame and fire segmentation [15,55,56], as well as in other energy-related applications [57]. Using neural networks for segmentation offers greater flexibility than traditional image processing methods, particularly in scenarios where real-time results are required. Neural networks can significantly accelerate the segmentation process, ensuring timely outcomes. Moreover, the need for preprocessing flame images, particularly those with low brightness, is reduced. The selection of the U-Net for this study was based on its recognized strength in pixel-accurate semantic segmentation. Although other modern architectures like YOLO [58] have been extended for segmentation tasks (YOLO-seg), they are fundamentally optimized for object detection and real-time speed [59], often at the cost of precise boundary detection. For flame image analysis, where accurately capturing the irregular and turbulent edges is critical for subsequent feature extraction, encoder-decoder networks like U-Net are generally more appropriate. Nevertheless, the complementary strengths of the two architectures suggest the potential for a combined framework, as discussed in previous studies [60].

The training dataset was generated from the ground truth images (See Section 3.2). Around 12,000 images from the three fuels were used to train and validate (20 % for validation) the U-Net, and around 18,000 were used for testing. Using a validation set helps fine-tune the model's parameters and assess its performance during training. At the same time, testing provides a final evaluation of the model's generalization ability on completely unseen data. To avoid bias, the entire dataset was shuffled before it was randomly split into training, validation, and test sets. The test dataset included samples of all three fuel types (natural gas, coal, and diesel), as well as samples from different test runs, showing different temporal variations. This ensured that the test evaluation reflected the dynamic behavior of flames in various conditions, rather than being limited to a single condition.

Several preprocessing steps were applied, including converting the images to grayscale, normalizing the pixel values to a range between 0 and 1, and shuffling the dataset to ensure randomness. A batch size of 8 was utilized during training, accompanied by a learning rate of 0.001, with the training process spanning 300 epochs. Mean squared error (MSE) was used as the loss function, and model performance was monitored by tracking both the training and validation loss to prevent overfitting. The importance of using deep learning techniques is that they do not need any preprocessing steps to obtain the results, which makes this approach suitable for real-time flame monitoring systems.

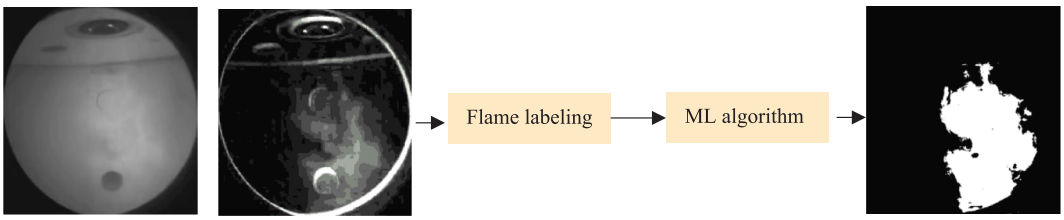

Fig. 4. The ground truth generation process.

The proposed network architecture comprises an encoder-decoder framework influenced by a U-Net structure designed for image processing tasks. The encoder section features convolutional layers followed by max-pooling operations, gradually increasing the depth of feature maps to capture intricate image features effectively. Meanwhile, the bottleneck layer condenses the learned features. The decoder section employs up-sampling layers to restore the spatial dimensions while concatenating feature maps from the encoder, allowing for precise localization. Finally, a convolutional layer with sigmoid activation generates the RGB color output. This architecture promotes both feature extraction and high-fidelity image reconstruction. The detailed network architecture is described as follows:

- Input Layer: Receives input data with a specified shape.
- Encoder Convolutional Layers: Extract features from the input image through convolution operations with ReLU activation, gradually increasing the depth to 64 and 128 channels while preserving spatial information via padding.
- Encoder Pooling Layers: Down-sample the feature maps using max-pooling with a 2x2 window to capture dominant features efficiently.
- Bottleneck Convolutional Layer: This layer condenses the learned features into a high-level representation with 256 channels, facilitating efficient information encoding.
- Decoder Up-Sampling Layers: Restore spatial dimensions through up-sampling operations with a 2x2 kernel size to match the original input dimensions.
- Decoder Concatenation Layers: Fuse feature maps from the corresponding encoder layers to facilitate precise localization of features during reconstruction.
- Decoder Convolutional Layers: Further refine the feature maps with convolution operations and ReLU activation, gradually decreasing the depth to 128 and 64 channels while maintaining spatial information.
- Output Convolutional Layer: This layer produces the final RGB color output with three channels using a convolutional layer with sigmoid activation, ensuring pixel-wise color prediction.

3.2. *Measuring the segmentation quality*

Evaluating the quality of the segmentation result is very important. There are two ways to assess it: subjective (visual) evaluation and objective evaluation. Visual evaluation is complex, as it can vary significantly from one human to another. Therefore, it requires an expert to do this task. The second type is called objective evaluation, and a ground truth image should be obtained manually. Then, the segmented results are compared with this reference image, including Intersection

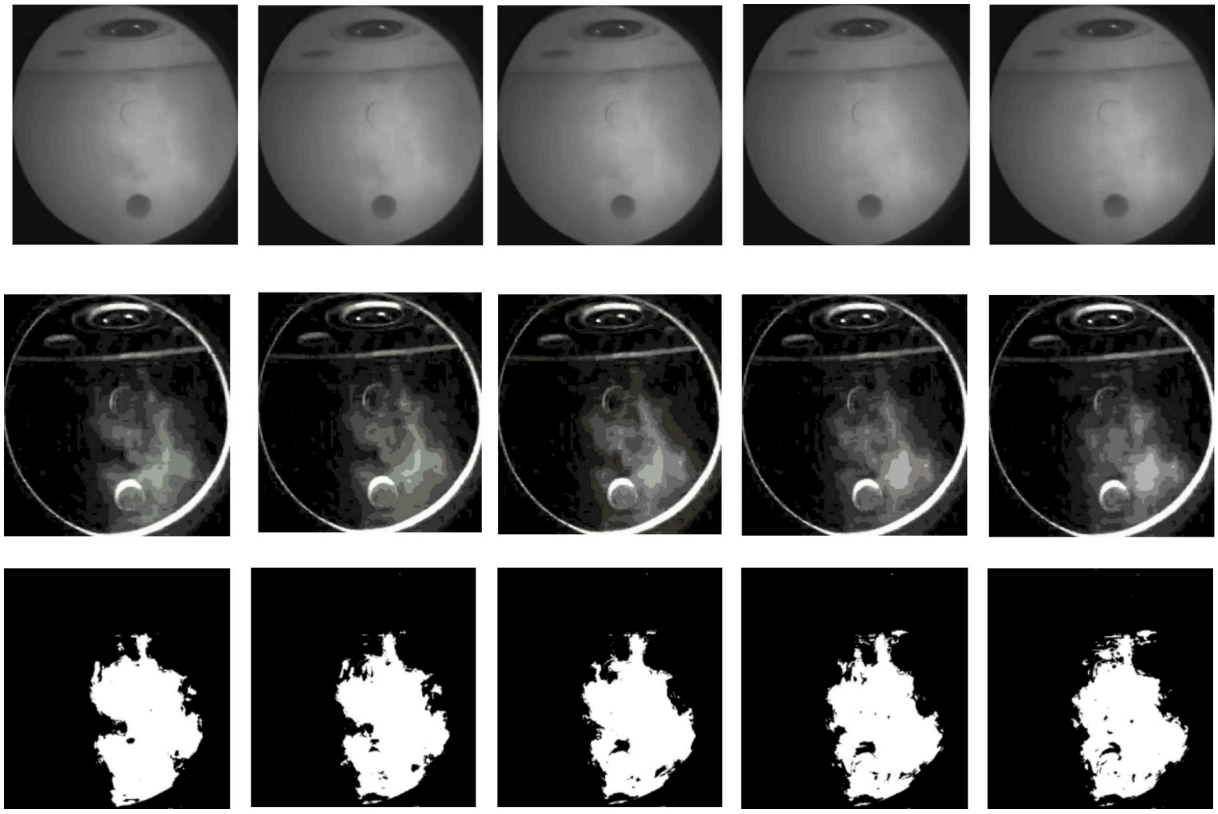

Fig. 5. The segmentation results of five successive images. Top: the original flame image. Middle: the processed frames. Bottom: The ground truth frames.

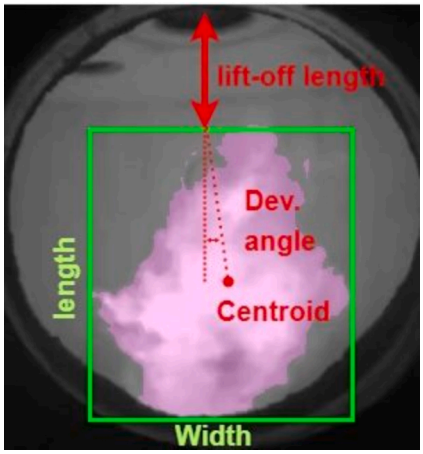

Fig. 6. Representation of the flame characteristics.

over Union (IoU) against ground truth and root mean square error (RMSE) for extracted geometric features. This combined approach ensures that the evaluation is supported by both subjective and objective measures. In this study, the ground truth of the solid and liquid fuel flames was obtained from manual thresholding, as the flame was clear in both cases.

The segmentation of gas fuel flame presents challenges in comparative analysis due to the absence of an established ground truth. Thus, the creation of ground truth becomes essential for accurate segmentation assessment. Fig. 4 illustrates the methodology employed to generate ground truth for low-brightness flames. The averaged background is initially subtracted from the image sequence to enhance flame visibility. Despite preprocessing efforts, segmentation remains challenging, as specific regions within the reactor exhibit brightness levels similar to the flame. To solve this, a manual labeling tool was utilized to distinguish flame regions from the background, encompassing areas with elevated brightness. Subsequently, a machine learning model was used to automate flame region extraction, streamlining the segmentation process. It is crucial to highlight that this process can serve as a standalone segmentation method. However, this method is suitable for offline segmentation of flames under specific conditions; therefore, it is unsuitable for online analysis. This limitation is noteworthy, particularly concerning the necessity for a more precise monitoring system, which often requires real-time data processing and analysis. The ground truth data for the three types of flames were used to train the U-net and also to evaluate the segmentation quality. However, it is important to note that any change in operating conditions will change the flame appearance and, consequently, the ground truth. Therefore, retraining the model with the updated ground truth images could be essential. Alternatively, it can be beneficial to generate a comprehensive dataset that encompasses a wide range of experimental conditions, including variations in operating parameters and camera settings. Training the neural network on this diverse dataset will enhance its ability to generalize across different scenarios within the same test facility, ultimately improving its adaptability and segmentation accuracy under varying conditions. Fig. 5 displays the segmentation results of five successive frames (gas fuel flame), demonstrating the method's ability to highlight and accurately segment the flame region to produce the ground truth.

After generating the ground truth, the Intersection over Union (IoU) metric was employed to evaluate the quality of the segmentation. IoU measures the extent of overlap between the predicted segmentation and the ground truth, providing a quantitative measure of how accurately the model identifies the target objects in the images. It is calculated by dividing the intersection area between the predicted and ground truth regions by the area of their union. A higher IoU score indicates a better correspondence between the predicted and ground truth segmentations, indicating improved accuracy of the segmentation algorithm. The IoU score, calculated as the ratio of the intersection area to the union area, quantifies the degree of overlap between the segmented regions and the ground truth as shown in the following equation:

$$\mathrm{IOU} = \frac{|\text{Area of Intersection}|}{|\text{Area of Union}|} \tag{7}$$

3.3. Extracting the geometric flame characteristics

The post-segmentation analysis of the flame images provided valuable insights. Firstly, we extracted instantaneous geometric flame parameters, including length, maximum width, ignition point, area, flame centroid, and deviation angle, as illustrated in Fig. 6. To achieve this, an in-house tool was developed in Python, utilizing libraries such as OpenCV for image processing, NumPy for numerical operations, and Pandas for data handling. This algorithm operates on the contours of the segmented flame mask to automate the feature extraction process. A minimum bounding rectangle is first fitted around the detected flame contour to standardize orientation and simplify geometry extraction. Based on this, the parameters are defined and calculated as follows:

- Flame length: The vertical distance between the topmost and bottommost points of the flame contour.
- Maximum width: The maximum horizontal span within the flame mask at any horizontal level.
- Ignition point: The center of the burner tip [5].
- Flame area: The total number of pixels within the segmented flame mask, converted to mm^2 using calibration.
- Flame centroid: The center of mass of the flame contour, calculated from the pixel distribution.
- Deviation angle: The angle between the vertical axis and the line connecting the ignition point to the flame centroid, representing flame oscillation.

It is important to note that flames are inherently three-dimensional; however, using two-dimensional image projections is a well-established and valid technique for estimating flames' features, e.g., length and surface area. The symmetry of flames, especially in controlled environments, allows 2D projections to capture accurate key features like flame length and boundary. Since flames are often optically transparent, their outer contours are easily detected in 2D images, making this method effective for real-time measurements. In many combustion systems, the flame's height extends predominantly along one axis; therefore, capturing its full extent in 2D is often sufficient. This technique is widely used in the literature, as shown in [1,14,15].

3.4. Flame stability assessment

This work presents a flame stability assessment methodology to demonstrate an application of the extracted flame characteristics. Unlike existing techniques in the literature, our method incorporates flame orientation and geometric parameters, making it more flexible and robust. By integrating these essential aspects, our approach offers a broader scope of analysis and greater resilience in assessing flame stability. The methodology quantifies the overall stability percentage by averaging the geometry, deviation angle, and lift-off (ignition point) stability indices.

The flame geometry stability index (GSI) starts with calculating the absolute percentage change (Δp_i) for length, width, and area, which is computed over successive frames $(i, i+1)$, representing the temporal variability of the flame dimensions. The index is then determined by combining the normalized average changes in height ($\overline{\Delta p_h}$), width ($\overline{\Delta p_w}$), and area ($\overline{\Delta p_a}$) with predefined weights (w_h, w_w, w_a). These weights are assigned to prioritize the significance of each geometric parameter in assessing flame stability, allowing for a balanced evalua-

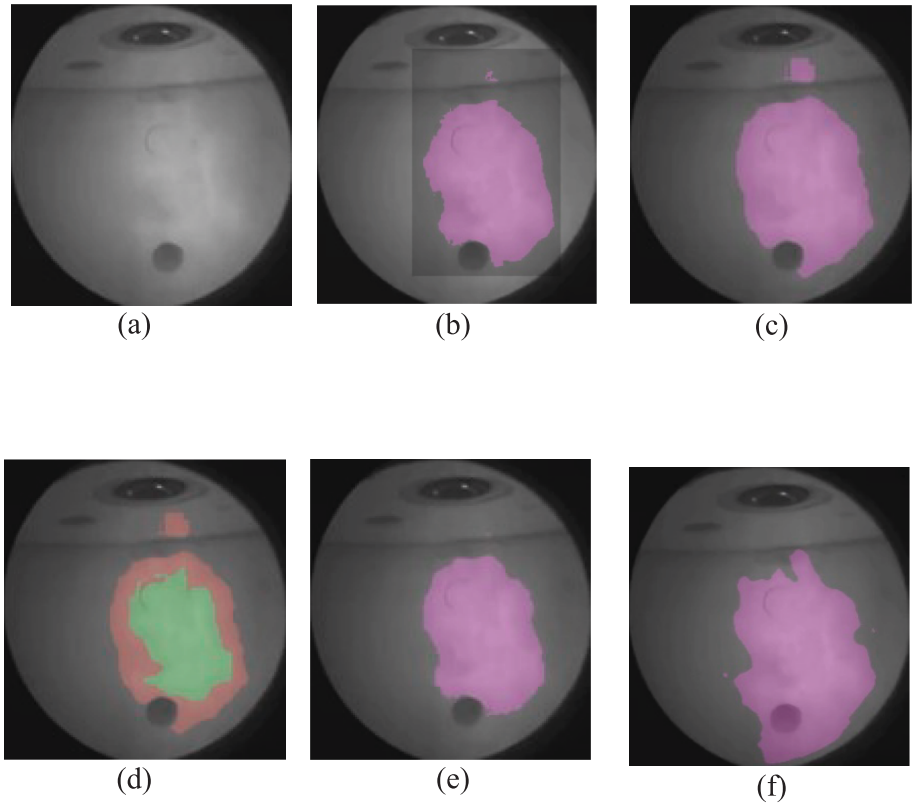

Fig. 7. A comparison between the different segmentation methods for gas fuel flame: a) Original image. b) Otsu's method. c) Manual thresholding $T = 130$. d) Multi level thresholding $T = [130, 150]$. e) KNN. f) U-Net.

tion of flame characteristics. The mathematical expressions can be found in Equations (8)–(10). Unlike the existing methods [61,62], which assume equal weightings for individual flame parameters, this assumption may not be valid in practice. A higher weighting should be given to the parameter, which is more sensitive to the change in flame stability [63]. For example, a flame in one frame may have the same area as in the next frame but exhibit different height and width, resulting in a completely different flame shape. In such cases, the weighting of parameters becomes crucial to prioritize which aspects are more significant for assessing flame stability. Another scenario is when a flame has a high Geometry Stability Index (GSI) but becomes detached from the burner tip, which indicates a different form of instability that could be overlooked under an equal-weighting assumption. Therefore, to develop a more flexible and accurate stability index, the weights must be adjusted to reflect the varying importance of each parameter.

$$\Delta p_i = \left| \frac{p_{i+1} - p_i}{\max(p_i, p_{i+1})} \right| \times 100\% \tag{8}$$

$$\overline{\Delta p_i} = \frac{\sum_{i=1}^{N} \Delta p_i}{N} \tag{9}$$

$$\mathrm{GSI} = 100\% - (w_{\mathrm{h}}.\overline{\Delta p_{\mathrm{h}}} + w_{\mathrm{w}}.\overline{\Delta p_{\mathrm{w}}} + w_{\mathrm{a}}.\overline{\Delta p_{\mathrm{a}}}) \tag{10}$$

For the flame stability based on the orientation and the position, the average deviation angle per frame ($\overline{\theta_i}$) and the average lift-off distance per frame ($\overline{L_i}$) are computed by summing the deviation angles and lift-off distances over the series of frames and dividing by the total number of frames (as shown in Equations (11) and (12)), denoted as N. These values represent the temporal variations in flame characteristics throughout the observation period. Subsequently, the Deviation Angle Stability Index (DASI) and Lift-off Stability Index (LOSI) are determined by normalizing the average deviation angle and average lift-off per frame, respectively, relative to their maximum possible values $\theta_{\max}$, and $L_{\max}$ (See Equations (13) and (14)). The maximum values for deviation angle and lift-off length serve as benchmarks representing the extreme ends of flame instability; thus, proximity to these values indicates a higher degree of instability, while deviation from them suggests greater flame stability. These indices provide insights into the temporal stability of the flame's orientation and position throughout the observation period.

$$\overline{\theta_i} = \frac{\sum_{i=1}^{N} \theta_i}{N} \tag{11}$$

$$\overline{L_i} = \frac{\sum_{i=1}^{N} L_i}{N} \tag{12}$$

$$\mathrm{DASI} = 100\% - \left(\frac{\overline{\theta_i} \times 100\%}{\theta_{\max}} \right) \tag{13}$$

$$\mathrm{LOSI} = 100\% - \left(\frac{\overline{L_i} \times 100\%}{L_{\max}} \right) \tag{14}$$

Finally, the overall stability percentage is calculated by combining the Geometry Stability Index (GSI) with the DASI and LOSI, weighted by predefined factors (w_{geometry}, w_{dev}, w_{liftoff}), and normalized by their sum (Equation (15)). This comprehensive approach offers a unified metric for evaluating flame stability, considering geometric parameters and temporal variations, and facilitates a nuanced understanding of the flame dynamics under study.

$$\textbf{Stability}\,\% = \frac{w_{\mathrm{geometry}}.\mathrm{GSI} + w_{\mathrm{dev}}.\mathrm{DASI} + w_{\mathrm{liftoff}}.\mathrm{LOSI}}{w_{\mathrm{geometry}} + w_{\mathrm{dev}} + w_{\mathrm{liftoff}}} \tag{15}$$

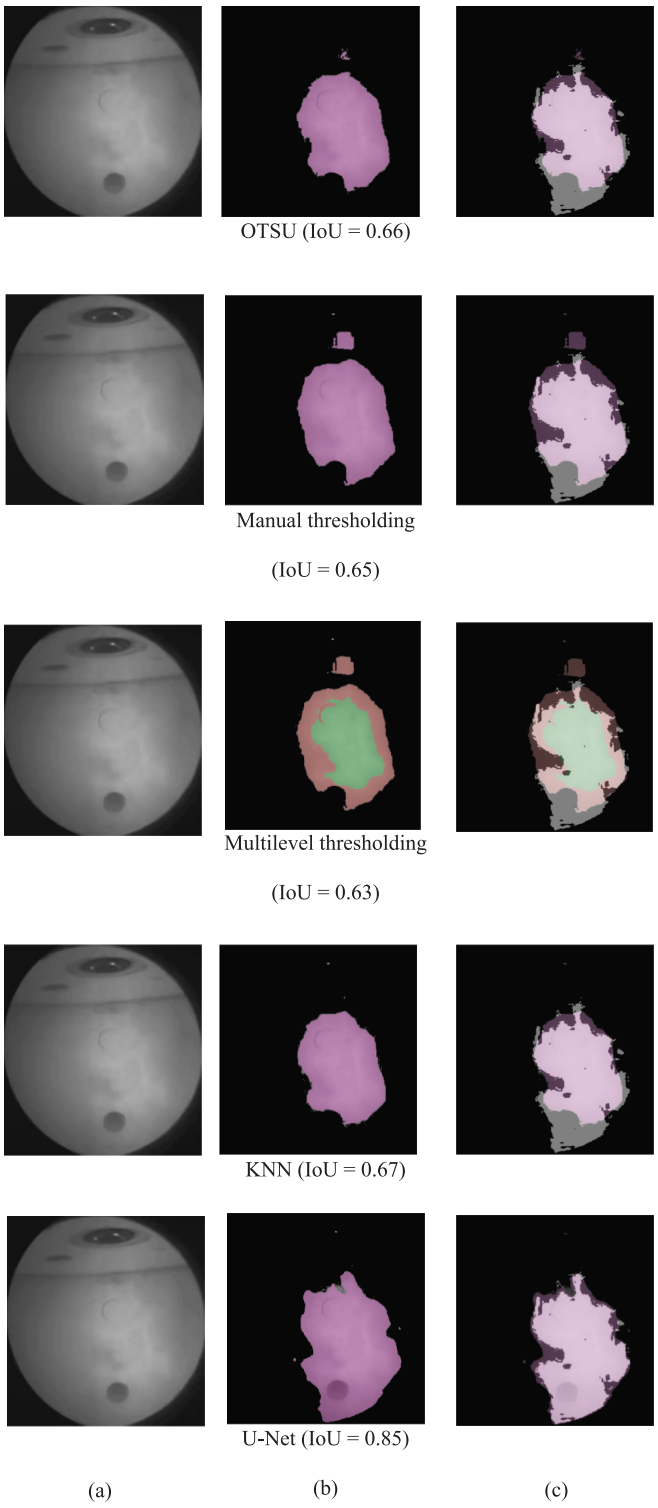

Fig. 8. Segmentation quality for gas fuel flame (a) Original flame image. (b) different segmentation results. (c) The intersection between the ground truth and the segmentation results (grey: ground truth, Purple, green, red: segmented flame).

4. Results and discussion

4.1. Instantaneous results

The study revealed distinct behaviors, shapes, stability, and brightness variations among flames from three feedstocks. Consequently, segmentation flexibility is a crucial criterion for selecting the most suitable algorithm for the provided data. Figs. 7, 9, and 10 show the segmentation results obtained using different methods for three distinct fuels. Notably, the gas fuel flame presents a considerable challenge in segmentation due to its low contrast against the background, as Fig. 7(a) shows. The OTSU method, depicted in Fig. 7(b), segmented the flame; however, a region of interest (ROI) must first be defined to obtain more accurate results (the dark region in Fig. 7(b)). Furthermore, manual thresholding (Fig. 7(c)) demonstrates improved results; however, adjusting the threshold value proves time-consuming and impractical for real-time applications, such as online flame systems. Multi-thresholding, employing two threshold values instead of one, provides enhanced insights into the flame but remains a time-consuming process requiring the adjustment of multiple thresholds. Finally, the KNN clustering method, utilizing 10 clusters, dynamically selects the best fit for flame borders, showcasing superior automation compared to other methods. This automated approach proves advantageous for efficient flame analysis, particularly in scenarios where real-time processing is essential. In terms of quality, U-Net consistently yields superior segmentation results, as visually depicted in Fig. 7(f). Furthermore, it eliminates the necessity for manual adjustment or preprocessing steps, making it ideal for real-time flame monitoring systems.

In this evaluation, the IoU was found to be 0.66 and 0.65 for Otsu and manual thresholding, indicating moderate agreement between the segmentation result and the ground truth. For the KNN algorithm, the IoU improved slightly to 0.67, suggesting a better alignment between the predicted and actual flame regions. Conversely, the multilevel thresholding approach yielded an IoU of 0.63, showing a slightly lower accuracy than the other methods. In this method, two threshold values (150 and 130) were employed to segment the flame. However, upon analysis, it was found that the flame edges corresponded to the threshold of 150 (indicated by the green region). The IoU scores provide quantitative insights into the performance of methods such as Otsu's thresholding, manual thresholding, multilevel thresholding, and KNN, guiding the selection of the most suitable approach for flame analysis applications. However, the flame shapes obtained from these methods often deviate from the actual flame shape, as shown in Fig. 8, making them inaccurate for segmenting low-brightness flames. This is because these methods primarily rely on identifying distinct intensity differences or optimal threshold values to separate objects from the background. However, in the case of gaseous fuel flames — characterized by low brightness and minimal contrast between the flame and the background — such differences are insufficiently pronounced. As a result, these methods fail to accurately distinguish flame regions, making them unsuitable for segmenting low-contrast gas flame images. On the other hand, deep learning methods provide an IoU of 0.85, demonstrating a significant improvement in accuracy and reliability, thus establishing them as the preferred choice for precise flame segmentation and analysis. A summary of the results is shown in Table 3.

Upon initial observation, it became evident that the solid fuel flame exhibits greater stability and higher brightness than the gas fuel flame, indicating increased soot content within the reactor. This characteristic simplifies the direct segmentation process, making it straightforward with conventional methods over time, as illustrated in Fig. 9. In this scenario, both the Otsu and KNN methods deliver optimal results, eliminating the necessity to fine-tune the threshold value for effective flame segmentation. It's worth noting that deep learning techniques not only deliver comparable quality to traditional image processing methods but also offer significantly faster processing times. This speed advantage makes them exceptionally well-suited for real-time applications.

A notable increase in flame instability occurs in the liquid fuel flame. This high instability makes it challenging to graphically determine the exact ignition point adequately, leading to the initiation of lift-off, as shown in Fig. 10. Furthermore, the flame's brightness diminishes, posing a challenge in precisely analyzing the flame front by distinguishing between grayscale values. Due to the bright background,

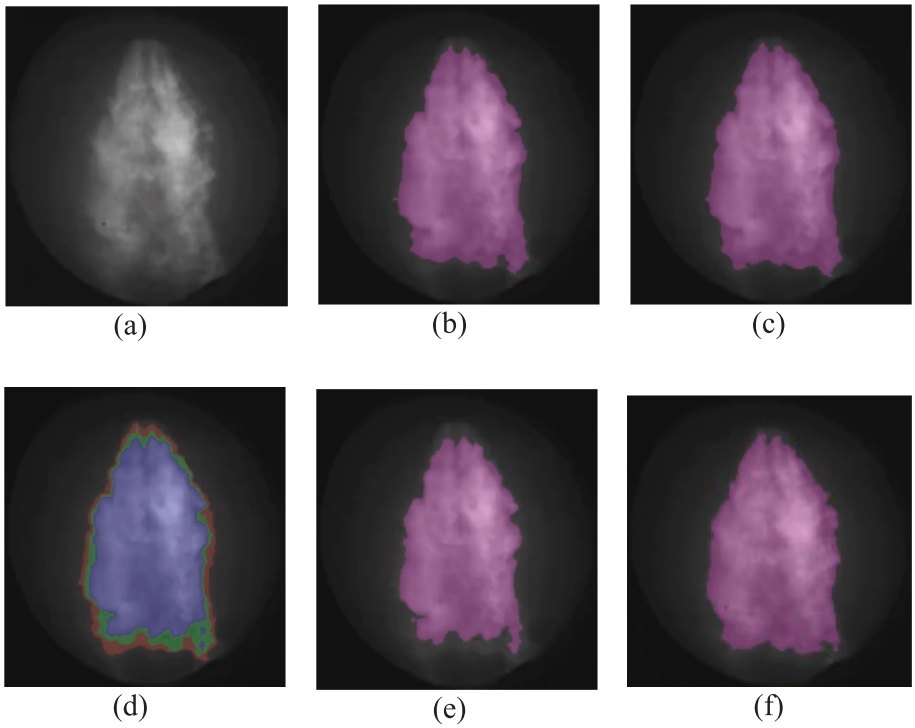

Fig. 9. A comparison between the different segmentation methods for solid fuel flame: a) Original image. b) Otsu's method. C) Manual thresholding $T = 70$. d) Multi level thresholding $T = [65, 75, 85]$. e) KNN. f) U-Net.

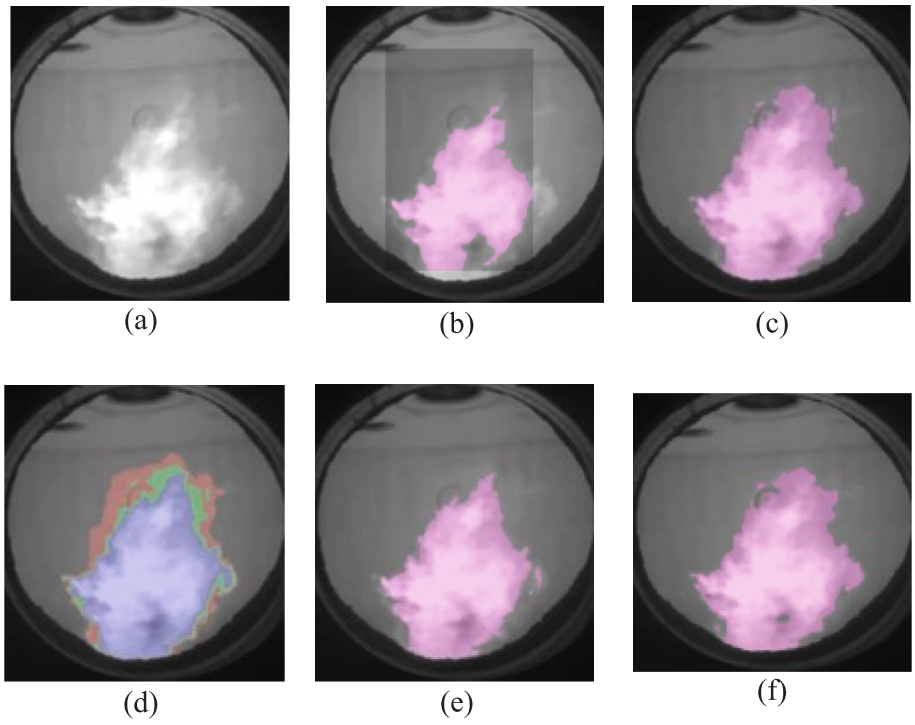

Fig. 10. A comparison between the different segmentation methods for liquid fuel flame: a) Original image. b) Otsu's method. C) Manual thresholding $T = 160$. d) Multi level thresholding $T = [150, 160, 170]$. e) KNN. f) U-Net.

Otsu's method struggled to differentiate between the flame and the background. However, using a predefined region of interest (ROI) improved the results, as shown in Fig. 10(b). KNN and U-Net stand out among the various methods employed as they visually provide the most accurate results. Table 4 summarizes the pros and cons of the segmentation algorithms. It is evident that manual thresholding is a time-consuming process and can vary significantly between operators. Additionally, threshold settings are easily influenced by changing operating conditions, leading to inconsistencies in the results. In contrast, employing deep learning with U-Net yields the most reliable

Table 3
IoU values for different methods.

Method	IoU
Otsu	0.66
Manual thresholding	0.65
Multi-level thresholding	0.63
KNN	0.67
U-Net	0.85

Table 4
A Comparative Overview of the segmentation algorithms.

Segmentation method	Flame type		Pros	Cons
OTSU	gas	x	• Automatic thresholding • Fast computation	• Assumption of bimodal distribution • Not suitable for images with low contrast between the background and objects • Sensitive to noise and variations in image quality
	solid	✓		
	liquid	✓		
Manual thresholding	gas	x	• Straightforward method • Fast computational time when the threshold is known	• Requires manual adjustment, which is time-consuming • Highly subjective and prone to operator variability • Assumes bimodal distribution, • Inconsistent results across different operators or conditions • Not adaptive to varying image conditions or changes in flame characteristics • May not perform well in images with low contrast or varying lighting conditions
	solid	✓		
	liquid	✓		
Multilevel thresholding	gas	x	• Adaptability to complex images • Handling of varied illumination • Capturing and distinguishing different structures or objects with varying intensities	• Increased Computational Complexity • Manual tuning: subjective and dependent on user expertise
	solid	✓		
	liquid	✓		
KNN	gas	x	• Applicability to Multiclass Segmentation • KNN is an instance-based learning algorithm, and it doesn't require a separate training phase • Simple Implementation • Robust to Noisy Data	• Computational Intensity • The choice of the number of neighbors (k) is critical, and selecting an inappropriate value may affect segmentation accuracy
	solid	✓		
	liquid	✓		
U-Net	gas	✓	• Works with low-brightness images • Very fast processing time • High accuracy	• Training requires extensive training data
	solid	✓		
	liquid	✓		

results, delivering highly accurate segmentation and effectively handling diverse flame qualities across various images. Furthermore, its fast processing time makes it exceptionally well-suited for real-time applications. Due to the limitations of traditional thresholding methods, the new approach, which combines a ground truth generation algorithm with the U-Net, proves to be a more flexible and robust solution for working with different flame images.

To strengthen the comparative analysis of flame segmentation methods, the performance of the proposed U-Net model was benchmarked against a state-of-the-art approach, YOLOv11-seg. The average Intersection over Union (IoU) across approximately 500 test cases for each fuel type confirmed the superior pixel-level accuracy of the proposed U-Net, which achieved IoUs of 0.95, 0.95, and 0.89 for coal, diesel, and natural gas fuel flames, respectively. In comparison, YOLOv11-seg yielded lower IoUs of 0.92, 0.85, and 0.78. This outcome is expected, as YOLO models are primarily optimized for object detection and real-time applications.

After segmentation, the next step involved extracting the instantaneous flame characteristics: height and width. This preliminary analysis provides a rapid assessment of how segmentation quality influences subsequent steps. Fig. 11 presents a visual comparison of flame height and width obtained through different segmentation algorithms across three flame instances. It is important to note that the ground truth for solid and liquid fuel flames results from manual thresholding. Table 5 quantitatively compares the root mean square error (RMSE) for the estimated flame height and width across different segmentation methods. The study revealed that segmentation accuracy significantly impacts the obtained flame characteristics. All algorithms exhibited discrepancies in height and width measurements in the low-brightness gas fuel flame scenario, highlighting the challenges in precisely defining exact flame boundaries. However, U-Net achieved an RMSE of 6.6 mm in height and 9.7 mm in width, significantly outperforming the traditional methods. This emphasizes the limitations of intensity-based segmentation techniques in low-contrast environments. Conversely, all algorithms demonstrated high agreement in height and width measurements for the high-brightness solid fuel flame. This indicates that even relatively simple segmentation methods can yield accurate results under favorable lighting conditions. The moderately bright liquid fuel flame presented an intermediate case, where acceptable consistency was observed among the algorithms, especially the U-net, although with slightly lower accuracy than the solid fuel flame results. These findings underscore the critical role of selecting appropriate segmentation algorithms based on the specific flame characteristics and image properties. For low-brightness flames, more sophisticated techniques that incorporate additional information beyond pixel intensity, such as texture, motion analysis, or deep learning, may be necessary to achieve reliable segmentation. Conversely, more straightforward intensity-based methods can provide satisfactory results for well-illuminated flames. However, deep learning methods have emerged as the preferred choice for applications demanding fast processing, such as real-time flame monitoring systems.

4.2. Flame stability assessment

Initially, equal weights were applied to calculate the stability indices to gather preliminary insights and determine how the weights should be prioritized. These tests were conducted on both solid and liquid fuel flames. The data showed that the solid fuel flame was much more stable than the liquid fuel flame, exhibiting significant fluctuations and detachment from the burner tip. As shown in Table 6, the geometry and deviation stability indices for the liquid fuel flame were both very high. However, visual observation indicated that this flame was unstable, as it remained consistently detached, reflected by its high lift-off stability index. Therefore, it became evident that the contribution of geometry and deviation angle should be reduced in the overall stability index to avoid overestimating the stability of flames in the current study. Only

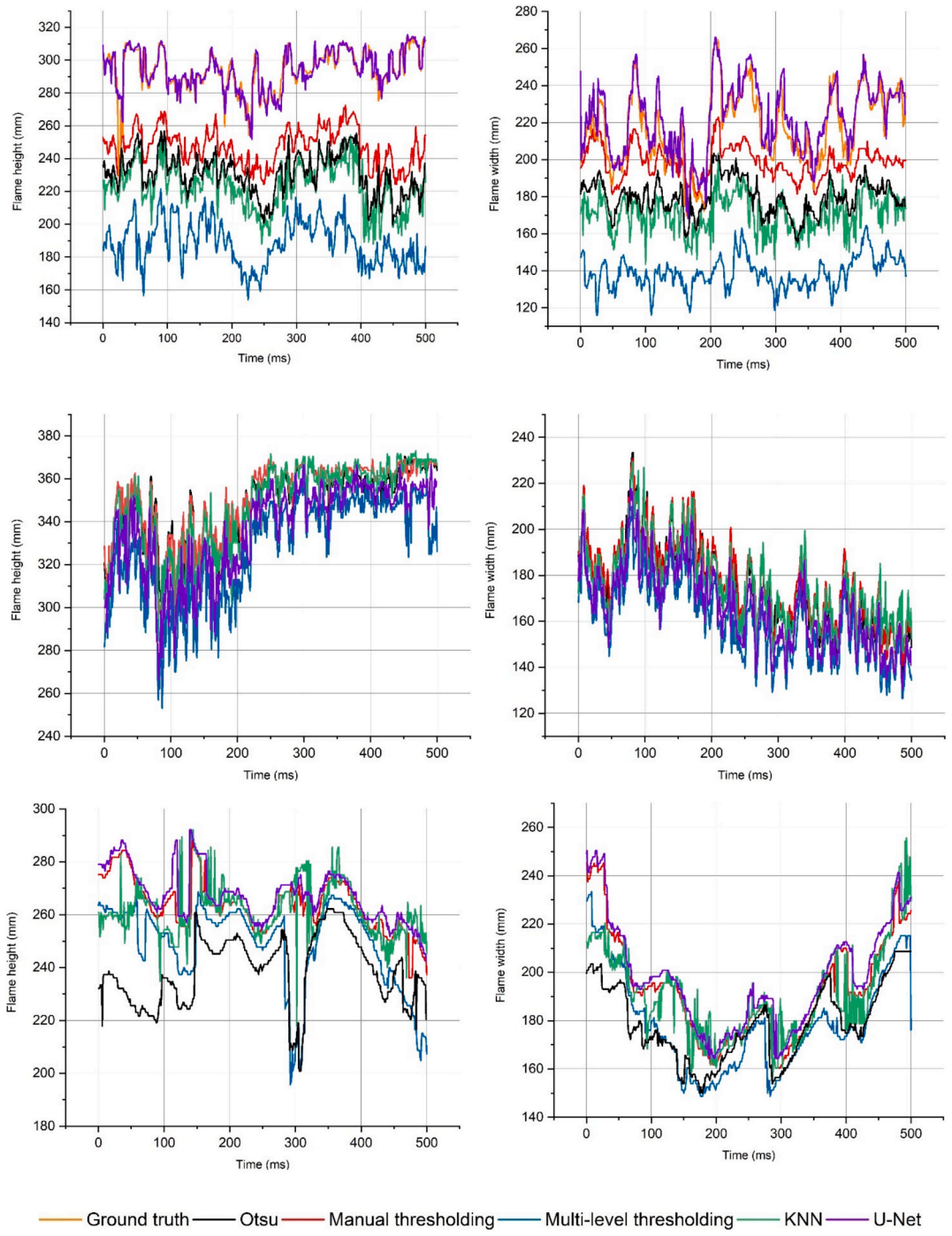

Fig. 11. Comparison between the flame height and width for the different flame types. Gas fuel flame (top). Solid fuel flame (middle). Liquid fuel flame (bottom).

solid and liquid fuel flames were included in this comparison, as their flame structures were visible in the images, enabling accurate and consistent extraction of key geometric features (e.g., length, width, ignition point), unlike the gas fuel flames. The liquid flame, in particular, exhibited lift-off behavior, which helps to illustrate the limitations of equal-weighting in the stability formula. These two contrasting cases provided sufficient variation to support the development and justification of the adjusted weighting strategy.

The next step involved slightly adjusting the weights to avoid overestimating the stability index and to make the method more adaptable to different conditions. As there are no available ground-truth values for flame stability, visual observation was used as a benchmark, and a two-stage sensitivity analysis was conducted to justify the weighting choices. In the first stage, the internal geometric weights (w_h, w_w, and w_a) were systematically varied from 0 to 1 in steps of 0.05, subject to the constraint that their sum equals 1, resulting in 84 distinct combinations. Across all these combinations, the GSI for solid (stable) and liquid (unstable) fuel flames differed by no more than 3.1 % (94.5–97.3 % for solid fuel vs. 92.9–94.9 % for liquid fuel), which confirms that geometric consistency alone cannot detect flame instability. For example, a detached flame may maintain stable dimensions, but it may be physically unstable. Nevertheless, geometry remains relevant because a truly stable flame must be attached (captured by LOSI) and shape-consistent (captured by GSI). Based on the analysis, the internal weights were fixed at $w_h = 0.4$, $w_w = 0.4$, and $w_a = 0.2$. This specific configuration was selected not because it maximized the difference between stable and

Table 5
Comparison of RMSE for different flame detection methods.

Method	Flame type	Height RMSE (mm)	Width RMSE (mm)
Otsu	gas	64	40.6
	solid	5.5	4.9
	liquid	28	18.8
Manual thresholding	gas	48.2	23.8
	solid	–	–
	liquid	–	–
Multi-level thresholding	gas	106	80.7
	solid	26	18.6
	liquid	20	17
KNN	gas	72.3	49.3
	solid	8.2	6.8
	liquid	10	11.3
U-Net	gas	6.6	9.7
	solid	17	14
	liquid	5.8	5.4

Table 6
Overview of the stability indices (equal weights).

Flame type	Length %	Width %	Area %	GSI %	Dev. angle %	Ignition point %	Overall SI %
Solid	97	94	96	**96**	97	98	**96**
Liquid	95	93	93	**93**	99	81	**90**

Table 7
Overview of the stability indices (different weights).

Flame type	GSI %	Dev. angle %	Ignition point %	Overall SI %
Gas	**96**	89	88	**90**
Solid	**96**	97	99	**98**
Liquid	**94**	99	81	**87**

unstable cases (2.1 %), but because it provides a balanced and physically interpretable weighting. The sensitivity analysis revealed that the absolute GSI values were relatively stable across the 84 combinations. Therefore, the choice of weights was guided by the principle that height and width are independent, primary descriptors of 2D flame morphology, whereas area is a derived parameter. Prioritizing height and width ensures that changes in flame shape (e.g., a transition from tall-narrow to short-wide) are adequately captured, which is crucial for generalizability across different fuel types and combustion regimes.

In the second stage, we varied the global weights for geometry (w_{geo}), deviation angle (w_{dev}), and lift-off stability ($w_{liftoff}$), while keeping the internal GSI weights fixed. The aim was to identify the weight set that would maximize the difference in the overall stability index between the stable (solid) and unstable (liquid) fuel flames, without relying on extreme, single-component weightings. Among all combinations, lift-off stability proved dominant: with $w_{liftoff} = 0.9$, the stability gap between solid (stable) and liquid (unstable) fuel flames reached 15.7 % (98.7 % vs. 83 %). In contrast, overemphasizing geometry ($w_{geo} = 0.9$) narrowed the gap to 2.6 %, while weighting the deviation angle too heavily ($w_{dev} = 0.9$), produced a physically invalid result because the detached liquid fuel flame scored higher than the attached solid fuel flame due to its narrow oscillation. Based on this analysis, we selected $w_{geo} = 0.2$, $w_{dev} = 0.2$, $w_{liftoff} = 0.6$, which provides strong diagnostic separation (10.4 % difference: 98.0 % vs. 87.6 %) while maintaining physical validity (stable > unstable).

The developed stability index was evaluated on the three main flame types. Results (See Table 7) show clear distinctions in stability across fuels: solid fuel flame achieved the highest overall stability (98 %), reflecting strong attachment and consistent behavior. Gas fuel flame showed moderate stability (90 %), while liquid fuel flame exhibited lower values of 87 % due primarily to reduced lift-off (attachment)

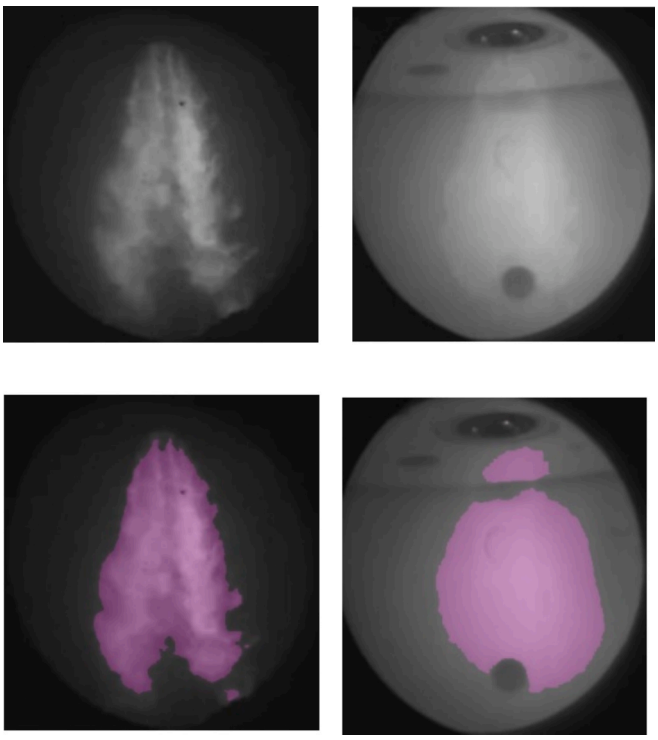

Fig. 12. Effect of low-brightness flames on the segmentation results.

stability (81 %). The proposed stability index integrates geometrical variation, deviation angle, and ignition point fluctuations to quantify temporal consistency in flame shape and attachment. This is directly linked to combustion, gasification, and any other process involving a flame. Low Lift-Off Stability Index (LOSI) values (<85 %, Table 7) indicate unstable ignition points, often preceding flame detachment or flameout [5], while excessive deviation angles can signal unstable combustion to acoustic oscillations. Likewise, consistent flame geometry (height, width, and area) generally reflects steady heat release, correlating with higher efficiency. By capturing these indicators in a single quantitative metric, the index provides relevance to key operational concerns such as efficiency, flameout risk, and acoustic instability. Furthermore, because the approach does not rely on fuel-specific assumptions, it is applicable to conventional as well as alternative feedstocks for combustion and gasification (e.g., ammonia, pyrolysis oil, bio-based fuels), providing a robust diagnostic tool for real-time monitoring and rapid operational adjustments in diverse industrial systems.

To explore further the impact of inaccurate segmentation on flame stability results, we focus on the solid fuel flame due to its distinct clarity compared to other flames. Consequently, its stability outcomes can be regarded as a baseline or "ground truth" for comparison. Subsequently, a scenario was created by replacing the background with a brighter alternative and reducing the flame brightness, as depicted in Fig. 12. This artificial condition allowed us to explore the implications of the results when the flame is not accurately delineated. It's evident that any change in the contrast between the flame and its background directly influences segmentation outcomes, thereby impacting the extracted characteristics. This influence is observable in the segmentation results.

In comparing the flame characteristics of the original flame to those of the artificial scenario, notable differences emerge. The artificial flame exhibits significantly higher percentages for length, width, and area stability, standing at 98 %, 99 %, and 99 %, respectively, in contrast to the original flame's respective percentages of 97 %, 95 %, and 96 % as shown in Table 8. This is because the segmented region is slightly constant. However, despite the significant change in the geometric stability, the artificial flame demonstrates a lower overall stability index (SI) of

Table 8
A Comparison between the original solid fuel flame stability and the artificial scenario.

Flame type	Length %	Width %	Area %	GSI %	Dev. angle %	Ignition point %	Overall SI %
Original	97	95	96	**96**	97	99	**98**
Artificial	98	99	99	**99**	88	84	**88**

88 % compared to the actual flame's SI of 98 %, as shown in Table 8. Notably, while the artificial decreases lift-off distance stability from 97 % to 88 %, its overall SI remains competitive due to enhancements in geometric parameters. These results serve as evidence and quantification of the inaccuracies that can arise when segmentation results are not precise. The comparison between the original and the artificial flame scenarios clearly demonstrates how variations in segmentation accuracy directly impact the quantification of flame stability characteristics.

5. Conclusion

In this study, two different aspects of flame diagnostics were undertaken. Firstly, a comparative analysis of various segmentation methods was conducted on three feedstocks (gas, solid, and liquid). The goal was to determine the best segmentation method for different flame types and conditions while addressing the critical challenge of low-brightness flame segmentation through our novel hybrid U-Net approach. This study also aimed to establish a comprehensive workflow for flame analysis that can be applied to future studies using alternative fuels. Therefore, well-known segmentation methods were employed to assess their performance under non-ideal flame image conditions. It was found that traditional image processing techniques, such as those used for low-brightness flames (e.g., gas fuel flames), failed to effectively detect the flame region, resulting in segmentation quality scores of 0.66 for Otsu, 0.65 for manual thresholding, 0.63 for multi-level thresholding, and 0.67 for KNN. This failure is primarily due to the inability of these methods to identify clear threshold values, as the intensity difference between the flame and the background was too low to enable accurate separation.

A new ground truth and U-Net-based method were used to address this issue, achieving a significantly higher IoU value of 0.89. Additionally, the flame shape was very close to the ground truth. For clear-appearance flames (e.g., solid and liquid flames), both deep learning and traditional image methods can perform the segmentation task; however, neural networks outperform them in processing time, as they require no threshold adjustment or optimization, making them highly flexible for various flame scenarios. It is acknowledged that the development and validation of the current model are based on a dataset limited to three fuel types operating under defined conditions within a single test facility. While the model demonstrates high performance with this data, its generalization capability must be tested with flames from a wider range of fuel types, test facilities, and operating conditions. Initial qualitative tests on different applications, including high-pressure partial oxidation and waste incineration, have yielded promising segmentation results. However, a comprehensive, quantitative evaluation is necessary, so this will be a primary focus for future research.

The second part of this study involved developing a new mathematical expression for flame stability based on the extracted flame characteristics to assess stability more comprehensively. This flame stability index assigns different weights to each flame characteristic, incorporating the geometric stability index (including flame height, width, and area), as well as the ignition point stability index and deviation angle stability index. The results indicated that the overall stability index of solid fuel flame was approximately 98 %, surpassing the stability indices of gas and liquid fuel flames, which were 90 % and 87 %, respectively. Finally, the impact of segmentation quality on the stability assessment was quantified by creating an artificial flame condition for the solid flame. It was found that, besides incorrect flame shape detection, the stability index had about a 10 % difference from the ground truth values. This integrated approach to flame analysis provides a robust framework for future studies, including those involving alternative fuels, demonstrating how advanced segmentation (U-Net) and weighted stability indices together overcome limitations of traditional methods in industrial environments.

CRediT authorship contribution statement

Mohsen Gharib: Writing – original draft, Software, Methodology, Conceptualization. **Markus Vogelbacher:** Writing – review & editing, Conceptualization. **Jörg Matthes:** Writing – review & editing, Supervision, Conceptualization. **Martin Gräbner:** Project administration. **Andreas Richter:** Writing – review & editing, Supervision, Project administration, Conceptualization.

Declaration of competing interest

The authors declare that they have no known competing financial interests or personal relationships that could have appeared to influence the work reported in this paper.

Acknowledgments

The authors gratefully acknowledge the co-financial support provided by tax funds based on the budget adopted by the Saxon State Parliament in the framework of Kohlenstoff-Kreislauf-Technologien, as well as the Federal Ministry for Economic Affairs and Climate Action, in the framework of "VERENA", Project no. 03EE5044C.

Data availability

The data that has been used is confidential.

References

[1] A. Richter, et al., A large-scale benchmark for the CFD modeling of non-catalytic reforming of natural gas based on the Freiberg test plant HP POX, Fuel 152 (2015) 110–121.
[2] M. Chimenti, et al., An IR image processing approach for characterising combustion instability, Infrared Phys. Technol. 46 (1-2) (2004) 41–47.
[3] T. Qiu, Y. Yan, Lu. Gang, An autoadaptive edge-detection algorithm for flame and fire image processing, IEEE Trans. Instrum. Meas. 61 (5) (2011) 1486–1493.
[4] Y. Yu, et al., Techniques and challenges of image segmentation: A review, Electronics 12 (5) (2023) 1199.
[5] M. Gharib, et al., Flame lift-off detector based on deep learning neural networks, Combust. Flame 260 (2024) 113215.
[6] J. Matthes, et al., A High-Speed Camera-Based Measurement System for the High-Pressure Entrained-Flow Gasification, Chem. Eng. Technol. 45 (12) (2022) 2313–2322.
[7] Zhang, Junzhen. "Computer image processing and neural network technology for thermal energy diagnosis of boiler plants." Thermal Science 24.5 Part B (2020): 3221-3228.
[8] A. González-Cencerrado, B. Peña, A. Gil, Coal flame characterization by means of digital image processing in a semi-industrial scale PF swirl burner, Appl. Energy 94 (2012) 375–384.
[9] J. Lukas, et al., Image-based biomass characterization: Comparison of conventional image processing and a deep learning approach, Fuel 341 (2023) 127705.
[10] M. Caponi, et al., Viscosity prediction using image processing and supervised learning, Fuel 339 (2023) 127320.
[11] W.G. Yan, C.J. Wang, J. Guo, One extended OTSU flame image recognition method using RGBL and stripe segmentation, Appl. Mech. Mater. 121 (2012) 2141–2145.
[12] X. Zhang, T. Yang, N. Cui, Flame image segmentation based on the bee colony algorithm with characteristics of levy flights, Math. Probl. Eng. 2015 (1) (2015) 805075.

[13] Šabanović, Adnan, et al. "Early Stage Flame Segmentation with DeepLabv3+ and Weighted Cross-Entropy." 2023 XXIX International Conference on Information, Communication and Automation Technologies (ICAT). IEEE, 2023.
[14] T. Imamura, et al., "Flame height of a turbulent diffusion jet flame with a comparatively high initial discharging velocity." Fire, Sci. Technol. 29 (1) (2010) 15–26.
[15] C. Pérez-Guerrero, et al., Experimental large-scale jet flames' geometrical features extraction for risk management using infrared images and deep learning segmentation methods, J. Loss Prev. Process Ind. 80 (2022) 104903.
[16] G.L. Hu, X.i. Jiang, Early fire detection of large space combining thresholding with edge detection techniques, Appl. Mech. Mater. 44 (2011) 2060–2064.
[17] A.KK. Wong, N.K. Fong, Experimental study of video fire detection and its applications, Procedia Eng. 71 (2014) 316–327.
[18] J. Chen, Q. Bao, Digital image processing based fire flame color and oscillation frequency analysis, Procedia Eng. 45 (2012) 595–601.
[19] Wang, Yuanbin, and Jieying Ren. "Low-light forest flame image segmentation based on color features." Journal of Physics: Conference Series. Vol. 1069. No. 1. IOP Publishing, 2018.
[20] Pérez-Guerrero, Carmina, et al. "Comparing machine learning based segmentation models on jet fire radiation zones." Advances in Computational Intelligence: 20th Mexican International Conference on Artificial Intelligence, MICAI 2021, Mexico City, Mexico, October 25–30, 2021, Proceedings, Part I 20. Springer International Publishing, 2021.
[21] P. Fan, et al., Experimental study of the impinging flame height in an opposed multi-burner gasifier, Energy Fuel 28 (8) (2014) 4895–4904.
[22] Li, Yuyan, and Lin Wang. "Flame Image Segmentation Algorithm Based on Motion and Color Saliency." Communications, Signal Processing, and Systems: Proceedings of the 2018 CSPS Volume II: Signal Processing 7th. Springer Singapore, 2020.
[23] J. Grosskopf, et al., Evaluation of deep learning-based segmentation methods for industrial burner flames, Energies 14 (6) (2021) 1716.
[24] Lundberg, Joachim, Mathias Henriksen, and André Vagner Gaathaug. "Using image processing for flame diagnostics." (2017).
[25] F. Tang, et al., Mean flame height and radiative heat flux characteristic of medium scale rectangular thermal buoyancy source with different aspect ratios in a sub-atmospheric pressure, Int. J. Heat Mass Transf. 84 (2015) 427–432.
[26] J.E. De León-Ruiz, et al., Image convolution-based experimental technique for flame front detection and dimension estimation: a case study on laminar-to-transition jet diffusion flame height measurement, Meas. Sci. Technol. 33 (7) (2022) 075406.
[27] S. Eckart, et al., Effects of Microwaves on Burning Velocity, UV–VIS-Spectra, and Exhaust Gas Composition of Premixed Propane Flames, Flow Turbul. Combust. 110 (3) (2023) 629–648.
[28] M.D. Takehara, Belo, et al., Pulverized biomass flame under imposed acoustic oscillations: Flame morphology and emission characteristics, Fuel Process. Technol. 238 (2022) 107484.
[29] S.R. Turns, Introduction to combustion, Vol. 287, McGraw-Hill Companies, New York, NY, USA, 1996.
[30] W. Yang, W. Blasiak, Chemical flame length and volume in liquified propane gas combustion using high-temperature and low-oxygen-concentration oxidizer, Energy Fuel 18 (5) (2004) 1329–1335.
[31] Z. Xi, et al., An investigation on flame shape and size for a high-pressure turbulent non-premixed swirl combustion, Energies 11 (4) (2018) 930.
[32] L.G. Zheng, et al., Measurement of flame height by image processing method, Adv. Mat. Res. 301 (2011) 983–988.
[33] Yu. Wang, et al., Pattern recognition for measuring the flame stability of gas-fired combustion based on the image processing technology, Fuel 270 (2020) 117486.
[34] Akintayo, Adedotun, et al. "Early detection of combustion instabilities using deep convolutional selective autoencoders on hi-speed flame video." arXiv preprint arXiv:1603.07839 (2016).
[35] T. Qiu, et al., An unsupervised classification method for flame image of pulverized coal combustion based on convolutional auto-encoder and hidden Markov model, Energies 12 (13) (2019) 2585.
[36] Z. Han, et al., Combustion stability monitoring through flame imaging and stacked sparse autoencoder based deep neural network, Appl. Energy 259 (2020) 114159.
[37] Chamberlin, D. S., and A. Rose. "The flicker of luminous flames." Proceedings of the Symposium on Combustion. Vol. 1. Elsevier, 1948.
[38] Y. Huang, et al., On-line flicker measurement of gaseous flames by image processing and spectral analysis, Meas. Sci. Technol. 10 (8) (1999) 726.
[39] Y.-C. Wu, et al., Novel methods for flame pulsation frequency measurement with image analysis, Fire Technol. 48 (2012) 389–403.
[40] Lu, Gang, et al. "Monitoring of oscillatory characteristics of pulverized coal flames through image processing and spectral analysis." IEEE transactions on instrumentation and measurement 55.1 (2006): 226-231.
[41] Matthes, Jörg, et al. "Camera-based Online Flame-Stability-Monitor for Load-Flexible Biomass Co-Combustion.".
[42] R.C. Gonzalez, Digital image processing, Pearson education india, 2009.
[43] I. Bankman (Ed.), Handbook of medical image processing and analysis, Elsevier, 2008.
[44] E.R. Davies, Computer and machine vision: theory, algorithms, practicalities, Academic Press, 2012.
[45] N. Otsu, A threshold selection method from gray-level histograms, Automatica 11 (285-296) (1975) 23–27.
[46] Z. Zhou, et al., Experimental study on determination of flame height and lift-off distance of rectangular source fuel jet fires, Appl. Therm. Eng. 152 (2019) 430–436.
[47] P. He, et al., The evolution of flame height and air flow for double rectangular pool fires, Fuel 237 (2019) 486–493.
[48] C. Tao, et al., The investigation of flame length of buoyancy-controlled gas fire bounded by wall and ceiling, Appl. Therm. Eng. 127 (2017) 1172–1183.
[49] Gao, Wei, et al. "Flame length of buoyant turbulent slot flame." Proceedings of the Combustion Institute 37.3 (2019): 3851-3858.
[50] H. Jia, J.U.N. Ma, W. Song, Multilevel thresholding segmentation for color image using modified moth-flame optimization, IEEE Access 7 (2019) 44097–44134.
[51] Abualigah, Laith, et al. "Moth-Flame Optimization Algorithm, Arithmetic Optimization Algorithm, Aquila Optimizer, Gray Wolf Optimizer, and Sine Cosine Algorithm: A Comparative Analysis Using Multilevel Thresholding Image Segmentation Problems." Handbook of Moth-Flame Optimization Algorithm. CRC Press, 2022. 241-263.
[52] Y. Wang, J. Ren, Application of knn algorithm based on particle swarm optimization in fire image segmentation, Journal of Electrical Engineering & Technology 14 (2019) 1707–1715.
[53] N.M. Zaitoun, M.J. Aqel, Survey on image segmentation techniques, Procedia Comput. Sci. 65 (2015) 797–806.
[54] Ronneberger, Olaf, Philipp Fischer, and Thomas Brox. "U-net: Convolutional networks for biomedical image segmentation." Medical image computing and computer-assisted intervention–MICCAI 2015: 18th international conference, Munich, Germany, October 5-9, 2015, proceedings, part III 18. Springer International Publishing, 2015.
[55] Y. Zheng, et al., Multi-scale semantic segmentation for fire smoke image based on global information and U-net, Electronics 11 (17) (2022) 2718.
[56] V.S. Bochkov, L.Y. Kataeva, WUUNET: Advanced fully convolutional neural network for multiclass fire segmentation, Symmetry 13 (1) (2021) 98.
[57] D. Gertsvolf, et al., A U-net convolutional neural network deep learning model application for identification of energy loss in infrared thermographic images, Appl. Energy 360 (2024) 122696.
[58] J. Redmon, et al., You only look once: Unified, real-time object detection. Proceedings of the IEEE conference on computer vision and pattern recognition, 2016.
[59] Mohamed, Eslam, et al. "Insta-yolo: Real-time instance segmentation." arXiv preprint arXiv:2102.06777 (2021).
[60] W.S. Mseddi, et al., Fire detection and segmentation using YOLOv5 and U-net. 2021 29th European Signal Processing Conference (EUSIPCO), 2021.
[61] D. Sun, Lu. Gang, Y. Yan, An embedded imaging and signal processing system for flame stability monitoring and characterisation. 2010 IEEE International Conference on Imaging Systems and Techniques, 2010.
[62] D. Sun, et al., A simple index based quantitative assessment of flame stability. 2013 IEEE International Conference on Imaging Systems and Techniques (IST), 2013.
[63] W. Xu, et al., Quantitative assessment of burner flame stability through digital image processing, IEEE Trans. Instrum. Meas. 71 (2022) 1–13.